Chinese Journal of Natural Medicines

Echinacoside targets HSC70 to promote osteoblast differentiation *via* Wnt/β-catenin signaling activation and mitochondrial regulation

Dong Han, Shihao Chen, Xiaojuan Wu, Xiaoli Jiang, Ping Li, Weilong Xu, Fei Li

Citation: Dong Han, Shihao Chen, Xiaojuan Wu, Xiaoli Jiang, Ping Li, Weilong Xu, Fei Li, Echinacoside targets HSC70 to promote osteoblast differentiation *via* Wnt/β-catenin signaling activation and mitochondrial regulation, Chinese Journal of Natural Medicines, 2026, 24(6), 734-744. doi: 10.1016/S1875-5364(26)61188-0.

View online: https://doi.org/10.1016/S1875-5364(26)61188-0

Chinese Journal of Natural Medicines 24 (2026) 734-744

Contents lists available at ScienceDirect

Chinese Journal of Natural Medicines

journal homepage: www.cjnmcpu.com/

Original article

Echinacoside targets HSC70 to promote osteoblast differentiation *via* Wnt/β-catenin signaling activation and mitochondrial regulation

Dong Han[a], Shihao Chen[a], Xiaojuan Wu[a], Xiaoli Jiang[a], Ping Li[a,*], Weilong Xu[b,*], Fei Li[a,*]

[a] *State key Laboratory of Natural Medicines, China Pharmaceutical University, Nanjing 211198, China*
[b] *Department of Endocrinology, Jiangsu Province Hospital of Chinese Medicine, Affiliated Hospital of Nanjing University of Chinese Medicine, Nanjing 210029, China*

ARTICLE INFO

Article history:
Received 12 September 2025
Revised 3 January 2026
Accepted 12 February 2026
Available online 20 June 2026

Keywords:
Echinacoside
HSC70
Osteoblast differentiation
Mitochondria
Osteoporosis

ABSTRACT

Osteoporosis (OP) is characterized by impaired osteoblast activity and excessive bone resorption, yet effective anabolic therapies remain limited. Here, we identify heat shock cognate 71 kDa protein (HSC70) as a novel negative regulator of osteoblast differentiation and reveal echinacoside (ECH), a natural phenylethanoid glycoside from *Cistanche deserticola*, as its direct inhibitor. Functional studies demonstrated that inhibition or knockdown of *Hsc70* promoted osteoblast differentiation and mineralization, while *Hsc70* overexpression abrogated the effects of ECH. Mechanistically, ECH suppressed HSC70 activity to activate Wnt/β-catenin signaling, enhance β-catenin nuclear translocation, and improve mitochondrial dynamics, ATP production, and biogenesis, thereby providing metabolic support for osteogenesis. *In vivo*, ECH treatment and *hsc70* knockout alleviated glucocorticoid-induced bone loss and restored mineralization in zebrafish models. Collectively, this work uncovers the HSC70–β-catenin/mitochondrial axis as a druggable pathway for skeletal homeostasis and positions ECH as a promising natural lead for developing bone-anabolic therapies against OP.

1. Introduction

Osteoporosis (OP) is the most prevalent metabolic bone disease, primarily affecting postmenopausal women. It is clinically defined by compromised bone mineral density (BMD) with elevated fracture susceptibility due to impaired microarchitectural integrity [1, 2]. Maintaining bone health relies on the dynamic equilibrium between bone resorption by osteoclasts and bone formation by osteoblasts [1]. The pathophysiological hallmark of OP is impaired osteogenic activity coupled with excessive osteoclastic resorption [2]. Consequently, targeting the bone remodeling process through the dual modulation of both anabolic and catabolic pathways represents a foundational strategy in regenerative approaches for OP management. Current treatments for OP aim to reduce susceptibility to osteoporotic fractures by either promoting bone formation or inhibiting bone resorption [3]. Pharmacological interventions primarily target osteoblasts or osteoclasts to alleviate symptoms [3, 4]. However, clinically available drugs that effectively promote bone formation or suppress bone resorption remain insufficient.

Heat shock cognate 71 kDa protein (HSC70/HSPA8) functions as a critical molecular chaperone essential for cellular homeostasis [5]. This constitutively expressed protein demonstrates multifaceted biological activities, including protein folding, transport, degradation, and clathrin-mediated endocytosis [5, 6]. Given its close association with the pathophysiology of various diseases, HSC70 is considered a promising therapeutic target [6]. Currently, relatively little research has examined the relationship between HSC70 and OP. Emerging evidence highlights a significant association between HSC70 dysregulation and bone metabolic disorders. For instance, Li et al. demonstrated that HSC70-mediated autophagic degradation of specific substrates plays a pivotal role in osteoclastogenesis and bone loss [7]. Moreover, the concurrent silencing of HSC70 and MNSFβ has been shown to inhibit RANKL-induced osteoclastogenesis [8]. These findings indicate that HSC70 is closely associated with osteoclastogenesis. However, no evidence indicates a direct association between HSC70 and osteoblast differentiation. Crucially, the functional activity of HSC70 is tightly regulated by its co-chaperones, such as the carboxyl terminus of Hsc70-interacting protein (CHIP) and BAG-1, which critically modulate its biological effects [6]. Evidence suggests that CHIP inhibits osteogenic differentiation by promoting ubiquitination-mediated degradation of Osterix and Runx2 [9, 10]. Unexpectedly, *Chip* knockout mice exhibit enhanced osteoclastogenesis alongside impaired osteoblast differentiation, resulting in significant bone loss [11]. Moreover, disruption of the BAG-1-HSC70 interaction markedly impairs the differentiation capacity of osteoblasts [12]. These results highlight that HSC70 is a promising target for OP therapy.

Echinacoside (ECH), a bioactive phenylethanoid glycoside from *Cistanche deserticola*, has demonstrated neuroprotective and anticancer activities in numerous studies [13-17]. Studies have shown that ECH can inhibit the formation and function of osteoclasts [18-20]. Our previous research also revealed that ECH enhances bone formation and reduces bone loss in ovariectomy (OVX) rats, highlighting its potential therapeutic efficacy against OP [21-23]. Despite these promising findings, the targets and exact

* Corresponding author.
E-mail addresses: liping2004@126.com (P. Li); xwl@njucm.edu.cn (W. Xu); lifei@cpu.edu.cn (F. Li)

https://doi.org/10.1016/S1875-5364(26)61188-0

mechanisms of ECH in OP treatment remain unclear. Small-molecule affinity chromatography represents a viable approach for drug target identification [24]. Natural products, with diverse bioactivities, have long served as invaluable resources for drug discovery and development [25]. It is worthwhile to discover naturally derived compounds that regulate bone remodeling to investigate their pharmacological targets and elucidate novel regulatory mechanisms in bone metabolism. Therefore, this study aimed to further evaluate the therapeutic effects of ECH on OP and elucidate its underlying molecular mechanisms by combining small-molecule affinity chromatography with *in vivo* and *in vitro* experimental research, ultimately providing a theoretical basis for the future pharmaceutical application of ECH.

In this study, we found that HSC70 is a direct cellular target of ECH. By targeting HSC70, ECH activates the Wnt/β-catenin signaling pathway and improves mitochondrial homeostasis, thereby promoting osteoblast differentiation and ultimately alleviating OP symptoms.

2. Materials and methods

2.1. Reagents and antibodies

Ascorbic acid (A5960) and β-glycerophosphate (G9422) were obtained from Sigma-Aldrich (USA). ECH (purity ≥ 98%) was purchased from Herbest Biotech (Baoji, China). Pronase E (P8360), Protease Inhibitor Cocktail (P001), Lipofectamine 2000 transfection reagent (11668019), and VER-155008 (HY-10941) were purchased from Solarbio (Beijing, China), NCM Biotech (Suzhou, China), Invitrogen (USA), and MCE (Shanghai, China), respectively. The antibodies are detailed in Supplementary Table 1.

2.2. Cell culture

MC3T3-E1 (Subclone 14) cells were acquired from Procell Biotech (Wuhan, China). The cells were cultured in MEM Alpha supplemented with 10% FBS and 1% penicillin-streptomycin at 37 °C with 5% CO_2 in a humidified environment.

2.3. Zebrafish

The feeding and breeding of zebrafish adhered to the standards outlined in the Zebrafish Book [26]. Adult male and female zebrafish were separately housed in a recirculating aquaculture system maintained at 28 °C under a 14-h light/10-h dark cycle and fed brine shrimp twice daily. The Animal Ethics Committee of China Pharmaceutical University authorized all experimental protocols (license number: SYXK (SU) 2016-0011; approval number: 2024-09-024).

Three-day post-fertilization (3 dpf) zebrafish larvae were randomly allocated into four experimental groups: the control group was maintained in embryo culture medium containing 0.1% DMSO; the model group was treated with 25 μmol·L^{-1} prednisolone (Pre); the model + etidronate disodium (Ed) group was treated with Pre and Ed (120 μmol·L^{-1}); the model + ECH group was treated with Pre and ECH (50/100/200 μmol·L^{-1}). Half of the medium was replaced daily over the entire 4-day treatment period. Subsequently, larvae were collected for enzyme activity and mineralization analysis.

2.4. Cell viability assay

The cytotoxic properties of ECH were evaluated *via* the CCK-8 assay following standard protocols. Briefly, cells were seeded into 96-well plates and then subjected to ECH treatment. After treatment, 10 μL of CCK-8 solution was added to each well and incubated at 37 °C for 2 h. Absorbance was then measured at 450 nm using a microplate reader, and cell viability was calculated relative to untreated controls.

2.5. Quantitative real-time PCR (qRT-PCR) analysis

Cellular RNA was extracted using RNA-easy Isolation Reagent (Vazyme, Nanjing, China), followed by cDNA synthesis via HiScript III All-in-one RT SuperMix (Vazyme). qRT-PCR was subsequently performed on a QuantStudio 3 Real-Time PCR System (Thermo Fisher Scientific, USA) using AceQ qPCR SYBR Green Master Mix (Vazyme). Relative mRNA levels were normalized to *Gapdh* (internal control) and calculated using the $2^{-\triangle\triangle Ct}$ method. Primer sequences are provided in Supplementary Table 2.

2.6. Alkaline phosphatase (ALP) activity assay

MC3T3-E1 cells were treated with ECH to induce osteoblast differentiation for 7 days. Following this incubation, cells were lysed, and ALP activity was measured using an ALP assay kit (Nanjing Jiancheng Bioengineering Institute, Nanjing, China).

2.7. ALP staining

MC3T3-E1 cells were treated with ECH to induce osteoblast differentiation for 7 days. Following this incubation, cells were fixed and subsequently stained using a TRAP/ALP Stain Kit (Wako, Japan). Stained cells were visualized and photographed (Nikon Ts2R, Japan).

2.8. Alizarin red staining

MC3T3-E1 cells were cultured for 21 days in osteogenic differentiation medium consisting of α-MEM enriched with 10 mmol·L^{-1} β-glycerophosphate, 50 μg·mL^{-1} ascorbic acid, and supplemented with ECH to induce mineralization. After fixation with 4% paraformaldehyde, cells were stained with Alizarin Red S solution at 37 °C for 30 min to visualize mineralization. The mineralization nodules, which stained red, were then visualized and photographed using a microscope (Nikon Ts2R, Japan).

Zebrafish larvae were fixed with 4% paraformaldehyde and subsequently decolorized for an hour with a solution containing 0.5% KOH and 3% H_2O_2. Following this, they were incubated in a solution containing 0.1% Alizarin Red and 0.5% KOH for 30 min. Larvae were then permeabilized overnight in permeabilization solution (0.5% KOH : glycerol = 1 : 1) and transferred to pure glycerol for storage. Skeletal morphology was documented using a stereo microscope (Olympus SZ61, Japan).

2.9. Biolayer interferometry (BLI) assay

The binding ability of ECH to HSC70 was analyzed using a ForteBio Octet Red 96 system (PALL, USA). Recombinant His-HSC70 protein was immobilized onto an NTA biosensor. Subsequently, the biosensors were incubated with serial concentrations of ECH in PBST. BLI data were analyzed using Data Analysis HT software.

2.10. Drug affinity responsive target stability (DARTS)

MC3T3-E1 cells were lysed using NP-40 Lysis Buffer. The lysate was then supplemented with ECH (50, 100 μmol·L^{-1}) and diluted to the same volume with 10 × TNC buffer (50 mmol·L^{-1} NaCl, 10 mmol·L^{-1} $CaCl_2$, 50 mmol·L^{-1} Tris-Hcl, pH 8.0). This mixture was incubated at 4 °C for 1 h. Subsequently, a 5 μg·mL^{-1} Pronase E solution was introduced, and incubation continued at room temperature for an additional 20 min. Following enzymatic

digestion, HSC70 was detected by immunoblotting with an anti-HSC70 antibody.

2.11. Cellular thermal shift assay (CETSA)

MC3T3-E1 cells were treated with ECH (50 μmol·L^{-1}) for 4 h at 37 °C. Following treatment, cells were harvested in PBS containing 1% protease inhibitor cocktail and divided into ten groups. They were heated for 3 min at gradient temperatures (43–61 °C) using a Veriti™ 96-Well Fast Thermal Cycler (ABI, USA). The samples were then subjected to repeated freeze–thaw cycles in liquid nitrogen. Cell lysates were detected by immunoblotting.

2.12. Knockdown of Hsc70 with siRNA

For the knockdown of *Hsc70* expression in cells, siRNA targeting *Hsc70* and siNC were synthesized by Suzhou Biosyntech Co., Ltd. (Suzhou, China) and then transfected into cells using Lipofectamine 2000 transfection reagent. The specific siRNA sequences used are detailed in Supplementary Table 3.

2.13. Mitro-Tracker staining

MC3T3-E1 cells were subjected to either ECH treatment or siRNA transfection for 48 h, followed by mitochondrial staining with 100 nmol·L^{-1} Mito-Tracker Green solution (Beyotime, Shanghai, China). Live-cell fluorescent images were subsequently captured using a confocal microscope (ANDOR, BC43, UK). Mitochondrial mean branch length was quantitatively analyzed using ImageJ (version 1.54f) with the MiNA 2.0 functional plugins.

2.14. Measurement of mtDNA content

Genomic DNA was extracted using the TIANamp Genomic DNA Kit (TIANGEN BIOTECH, Beijing, China). qRT-PCR was subsequently performed to determine the relative copy numbers of nuclear DNA (nDNA) and mitochondrial DNA (mtDNA). The primer sequences used for these analyses are detailed in Supplementary Table 4.

2.15. Western blot (WB) analysis

Lysates were prepared using a lysis buffer containing protease inhibitor cocktail. Protein quantification was performed using the BCA assay kit. Equal amounts of protein were denatured in 5× SDS-PAGE sample loading buffer by boiling at 100 °C for 5 min. Proteins were then separated by SDS-PAGE and subsequently transferred onto nitrocellulose membranes via wet transfer. Membranes were blocked in 5% non-fat milk for 2 h at room temperature, then probed with primary antibodies overnight at 4 °C. After three 10-min TBST washes, membranes were incubated with HRP-conjugated secondary antibodies at room temperature for 1 h, washed again with TBST, and finally visualized using a chemiluminescence imaging system (Tanon 5200, Shanghai, China).

2.16. Molecular docking

The 3D structure of HSC70 was retrieved from the PDB database (https://www.rcsb.org/, PDB code: 3M3Z), and the structure of ECH was sourced from the PubChem database (https://pubchem.ncbi.nlm.nih.gov/, PubChem CID: 5281771). Molecular docking and result visualization were performed using AutoDockTools (Version 1.5.7) and PyMOL (Version 2.5.0), respectively.

2.17. Statistical analysis

Statistical analysis was conducted using GraphPad Prism (Version 8.0.2). Two-tailed Student's *t*-test was used for comparison of two groups, and one-way ANOVA was used for comparison of multiple groups. Data were considered statistically significant when P was < 0.05.

3. Results

3.1. ECH promotes osteoblast differentiation in vitro

Promoting osteoblast-mediated bone formation is considered an effective approach to alleviate OP. Therefore, we initially explored the potential of ECH to stimulate osteoblast differentiation (Fig. 1A). After 72 h of ECH treatment, the viability of MC3T3-E1 cells showed only a slight reduction, suggesting that ECH had no obvious cytotoxicity (Fig. 1B). Osteoblast differentiation is mainly regulated by Runx2 and Osterix, which control the expression of bone formation marker genes such as type Ⅰ collagen (*Col1a1*) and osteocalcin (*Ocn*). ALP, a widely recognized biomarker for osteoblast differentiation, is also closely associated with the osteogenic process. qRT-PCR results revealed ECH significantly upregulated the mRNA levels of *Runx2*, *Osterix*, *Alp*, *Col1a1*, and *Ocn* (Figs. 1C–1G). Furthermore, both ALP staining and activity assays showed that ECH markedly increased ALP activity (Figs. 1H, 1I). Mineralization nodules form at the end of osteoblast differentiation. ECH notably increased the formation of mineralization nodules, as demonstrated by alizarin red staining (Fig. 1J). Altogether, our findings suggest that ECH effectively promotes osteoblast differentiation *in vitro*.

3.2. HSC70 serves as a cellular target of ECH

Cellular targets are the molecular basis of ECH-mediated bone homeostasis. To identify these targets, we developed ECH-conjugated epoxy-activated Sepharose beads 6B (ECH beads) as an affinity-based tool for isolating proteins that directly interact with ECH (Fig. S1). Subsequently, we performed Coomassie blue staining and liquid chromatography-tandem mass spectrometry (LC-MS/MS) to detect and identify the bound proteins (Fig. 2A). Notably, the abundance of HSC70 was particularly prominent among the identified proteins (Fig. 2B). Moreover, a multi-database integrated network pharmacology analysis was performed, which revealed 80 shared target genes as potential therapeutic targets of ECH for OP (Fig. S2A). Significantly, HSC70 (encoded by *HSPA8* or *HSC70*) emerged as one of the core targets within this network (Fig. S2B). Therefore, we hypothesized that HSC70 may function as a direct cellular target of ECH. Further experiments demonstrated that HSC70 was pulled down by ECH beads, while excess ECH competitively inhibited this interaction (Fig. 2C). Octet Biolayer Interferometry (BLI) revealed that ECH directly bound to HSC70 (Kd = 0.18 μmol·L^{-1}, Fig. 2D). Drug affinity responsive target stability (DARTS) analysis indicated that ECH increased the stability of HSC70 by enhancing its resistance to proteolysis (Fig. 2E). Additionally, ECH improved the thermal stability of HSC70, as demonstrated by the cellular thermal shift assay (CETSA) (Figs. 2F, 2G). To identify potential interaction sites and binding energy between ECH and HSC70, we performed molecular docking of ECH into the HSC70 structure (PDB code: 3M3Z) (Fig. 2H). Overall, these findings confirm that ECH directly binds to HSC70.

3.3. HSC70 inhibits osteoblast differentiation

To evaluate the potential role of HSC70 in the differentiation of MC3T3-E1 cells, we treated the cells with VER-155008, a po-

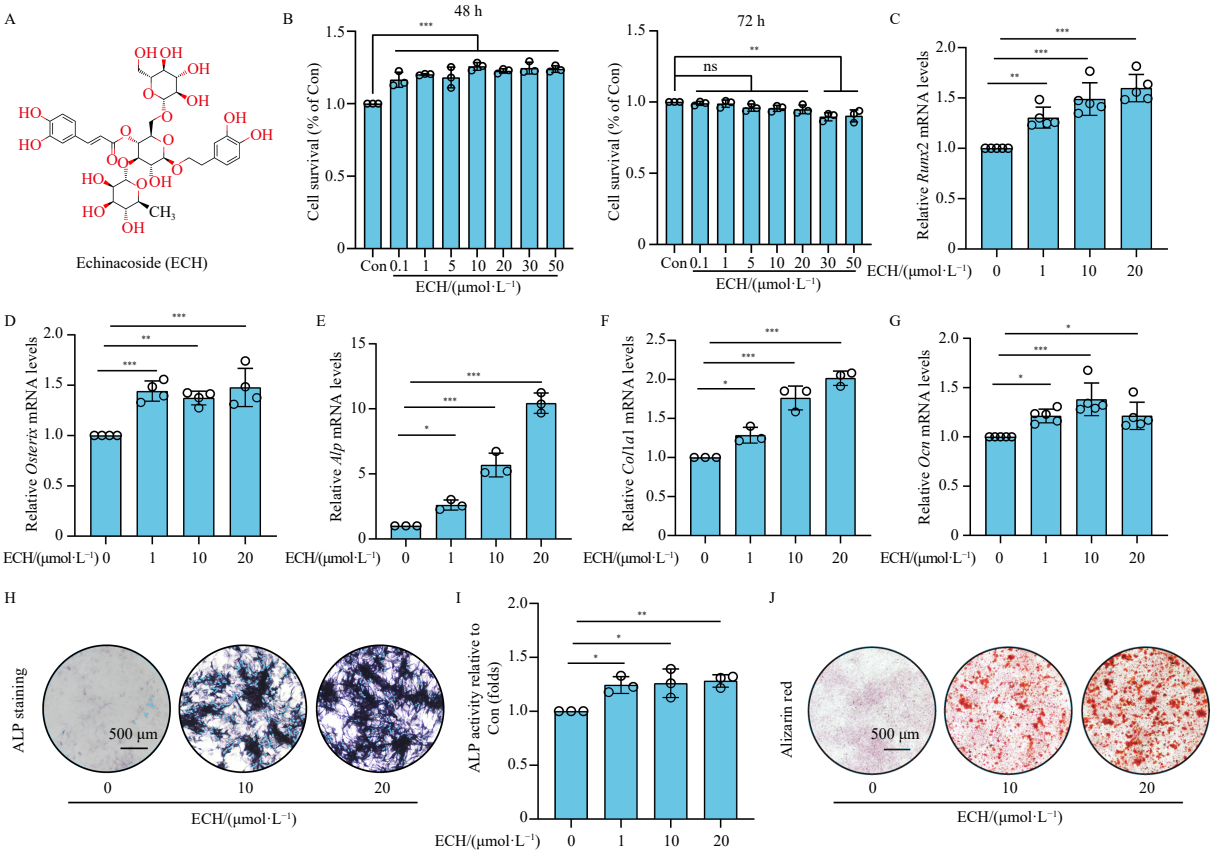

Fig. 1 ECH promotes osteoblast differentiation *in vitro*. (A) Chemical structure of echinacoside (ECH). (B) Effects of ECH on MC3T3-E1 cell viability after 48 h and 72 h of treatment. $n = 3$. (C-G) qRT-PCR analysis of *Runx2*, *Osterix*, *Alp*, *Col1a1*, and *Ocn* mRNA levels in MC3T3-E1 cells treated with ECH for 72 h. $n = 5$, 4, 3, 3, and 5, respectively. (H) Representative ALP staining images showing ALP activity in MC3T3-E1 cells treated with ECH for 7 days. Scale bar, 500 μm. $n = 3$. (I) Quantification of ALP activity in MC3T3-E1 cells treated with ECH for 7 days using an ALP assay kit. $n = 3$. (J) Representative Alizarin Red staining images showing mineralization in MC3T3-E1 cells treated with ECH for 21 days. Scale bar, 500 μm. $n = 3$. Data are expressed as means ± SD. $^{***}P < 0.001$, $^{**}P < 0.01$, $^{*}P < 0.05$ *vs* Control. ns, not significant.

tent HSC70 inhibitor. qRT-PCR analysis revealed that VER-155008 treatment upregulated several osteogenesis markers (Fig. 3A). Additionally, VER-155008 significantly increased ALP activity (Figs. 3B, 3C). Alizarin red staining demonstrated that VER-155008 significantly enhanced the mineralization nodule area (Fig. 3D). Moreover, *Hsc70* knockdown markedly promoted the expression of several osteogenesis markers, increased ALP activity, and enhanced mineralization nodule formation (Figs. 3E–3H). However, the enhanced expression of osteoblast differentiation-related transcription factors induced by ECH was reversed by *Hsc70* overexpression (Fig. 3I). Similarly, *Hsc70* overexpression also blocked the ECH-mediated increase in ALP activity and mineralization nodule formation (Figs. 3J–3L). Altogether, these results indicate that HSC70 inhibits osteoblast differentiation.

3.4. HSC70 regulates osteoblast differentiation through the Wnt/β-catenin signaling pathway

To elucidate the molecular mechanisms through which HSC70 influences osteoblast differentiation, we performed quantitative proteomic analysis on MC3T3-E1 cells, comparing the *Hsc70* knockdown group (si*Hsc70*) with a negative control (siNC). Principal component analysis (PCA) showed distinct clustering between the two groups, indicating significant proteomic differences (Fig. 4A). Differential protein expression analysis identified a total of 1561 significantly upregulated proteins and 1332 significantly downregulated proteins in the si*Hsc70* group relative to the siNC group (Figs. 4B–4C). Gene set enrichment analysis (GSEA) showed predominant downregulation of proteins associated with negative regulation of the canonical Wnt signaling pathway in *Hsc70*-deficient cells (Fig. 4D). Given the critical role of the canonical Wnt signaling pathway in bone formation, we systematically investigated its modulation by ECH and HSC70 in MC3T3-E1 cells. WB analysis indicated that ECH inhibited GSK3β activity by enhancing its phosphorylation at Ser9, thereby disrupting the β-catenin destruction complex and stabilizing β-catenin (Fig. 4E). Concurrently, ECH significantly promoted β-catenin nuclear translocation (Figs. 4F, 4G). Consistent with these findings, VER-155008 treatment also upregulated p-GSK3β (ser9) levels and enhanced β-catenin nuclear translocation (Figs. 4H–4J). Next, we assessed the effects of *Hsc70* knockdown or overexpression on the Wnt/β-catenin signaling pathway. *Hsc70* knockdown enhanced p-GSK3β (ser9) levels and facilitated β-catenin nuclear translocation (Figs. 4K–4M). Conversely, *Hsc70* overexpression abolished ECH-induced activation of the Wnt/β-catenin signaling pathway (Figs. 4N–4P). Altogether, these results demonstrate that HSC70 regulates osteoblast differentiation through the Wnt/β-catenin signaling pathway.

3.5. HSC70 regulates mitochondrial homeostasis for osteoblast differentiation

To further explore the biological mechanism of HSC70-mediated osteoblast differentiation, we conducted Gene Ontology (GO) enrichment analysis on the set of differentially expressed proteins identified in *Hsc70* knockdown MC3T3-E1 cells. The analysis revealed activation of mitochondria-related pathways (Fig. 5A). GSEA further demonstrated upregulated expression of mitochondrial proteins and enhanced mitochondrial energy metabolism (Figs. 5B–5E). Based on these results, we hypothesized that ECH, by inhibiting HSC70, may potentiate osteoblast differentiation through the augmentation of mitochondrial energy metabolism. First, we assessed mitochondrial morphology in ECH-treated

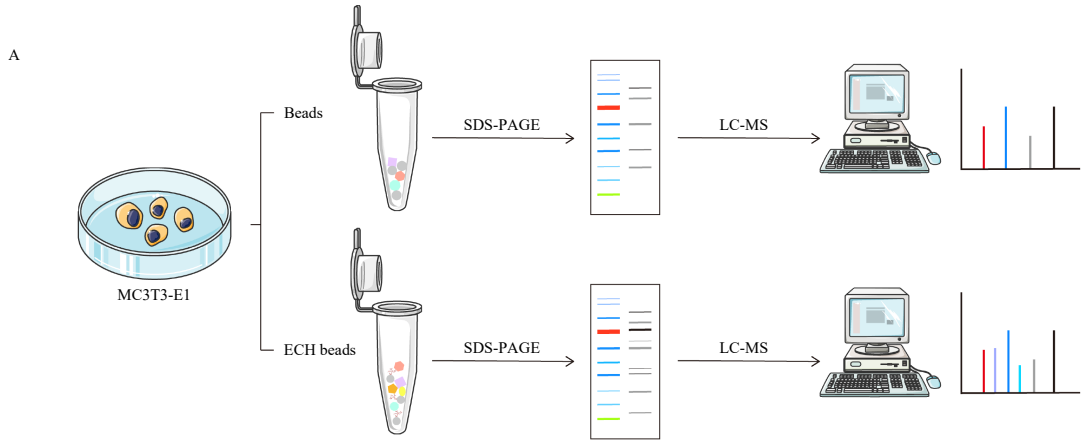

B

MC3T3-E1				
Accession		Gene symbol	MW/kDa	Abundance
No.1	Q03265	Atp5f1a	59.7	5 892 821 869
No.2	P63017	Hspa8/Hsc70	70.8	4 980 491 629
No.3	P56480	Atp5f1b	56.3	4 522 083 818
No.4	Q01853	Vcp	89.3	2 931 558 510
No.5	P06151	Ldha	36.5	2 801 310 404
No.6	P20029	Hspa5	72.4	2 650 817 523
No.7	Q01768	Nme2	17.4	2 376 999 533
No.8	P63038	Hspd1	60.9	2 288 124 205

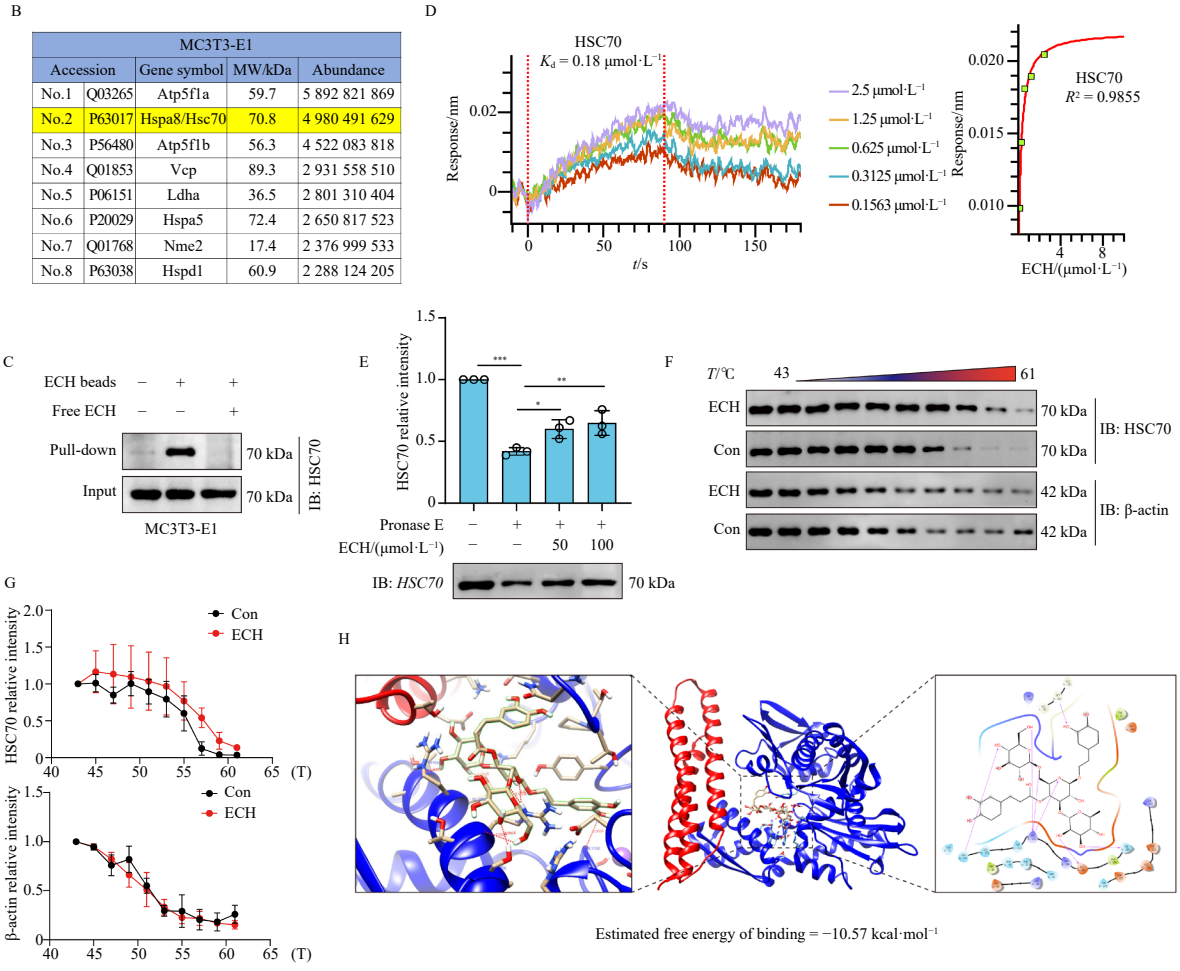

Fig. 2 HSC70 serves as a cellular target of ECH. (A) Schematic workflow for identifying cellular targets of ECH. (B) Top eight candidate proteins screened by LC-MS/MS in MC3T3-E1 cells as potential ECH-binding partners. (C) Pull-down assays demonstrating ECH binding to HSC70 in MC3T3-E1 cells. n = 3. (D) Binding kinetics of ECH to HSC70 analyzed by biolayer interferometry (BLI). (E) ECH enhances HSC70 resistance to proteolysis. n = 3. (F-G) ECH stabilizes HSC70 against thermal denaturation. n = 3. (H) Molecular docking model of ECH-HSC70 interaction (PDB: 3M3Z) with predicted binding energy. Data are expressed as means ± SD. $^{***}P < 0.001$, $^{**}P < 0.01$, $^{*}P < 0.05$ *vs* Control.

MC3T3-E1 cells. The results showed increased mitochondrial fragmentation and donut-shaped mitochondrial formation (Figs. 5F, 5G). Mitochondria are highly dynamic organelles in mammalian cells, and their functional integrity is regulated by coordinated fusion (mediated by OPA1 and MFN1/2) and fission (mediated by Drp1). The qRT-PCR analysis indicated that ECH treatment for 48 h upregulated *Drp1* mRNA levels and downregulated *Mfn2* mRNA levels (Fig. 5H). WB analysis confirmed increased Drp1 protein levels and decreased MFN2 protein levels (Fig. 5I). Moreover, ECH treatment significantly enhanced cellular ATP production and increased mitochondrial DNA (mtDNA) content (Figs. 5J, 5K). Among mitochondrial biogenesis markers (PGC-1α, ATP5B, and TFAM), ECH specifically upregulated TFAM expression, whereas it had no significant effect on PGC-1α or ATP5B levels (Fig. 5L). Consistently, *Hsc70* knockdown recapitulated ECH's effects on MC3T3-E1 cells: increased mitochondrial fragmentation and formation of donut-shaped mitochondria, elevated Drp1 and TFAM expression, reduced MFN2 expression, enhanced ATP production, and increased mtDNA content (Figs. 5M–5R). Collectively, these findings indicate that HSC70 regulates mitochondrial homeostasis for osteoblast differentiation.

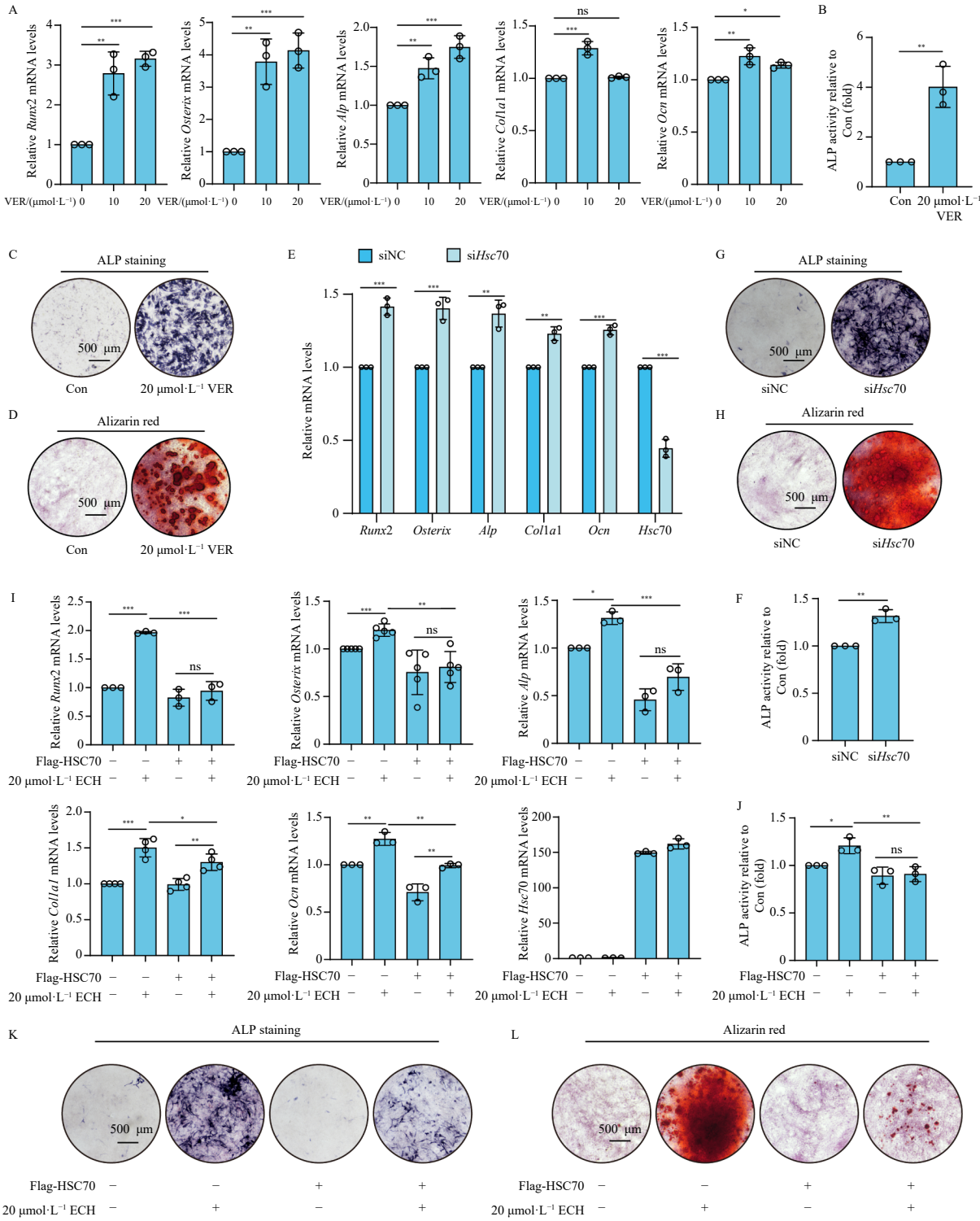

Fig. 3 HSC70 inhibits osteoblast differentiation. (A) qRT-PCR analysis of osteoblast differentiation markers (*Runx2*, *Osterix*, *Alp*, *Col1a1*, *Ocn*) in MC3T3-E1 cells treated with VER-155008 for 72 h. $n = 3$. (B) ALP activity quantification in MC3T3-E1 cells treated with VER-155008 for 7 days. $n = 3$. (C) Representative ALP staining images showing enhanced activity in MC3T3-E1 cells treated with VER-155008 for 7 days. Scale bar, 500 μm. $n = 3$. (D) Representative Alizarin Red staining images demonstrating mineralization in MC3T3-E1 cells treated with VER-155008 for 21 days. Scale bar, 500 μm. $n = 3$. (E) qRT-PCR analysis of osteoblast markers in MC3T3-E1 cells following *Hsc70* knockdown. $n = 3$. (F) ALP activity quantification in *Hsc70*-knockdown MC3T3-E1 cells. $n = 3$. (G) ALP staining images of *Hsc70*-knockdown MC3T3-E1 cells. Scale bar, 500 μm. $n = 3$. (H) Mineralization in *Hsc70*-knockdown MC3T3-E1 cells assessed by Alizarin Red staining. Scale bar, 500 μm. $n = 3$. (I) qRT-PCR analysis of osteoblast markers in MC3T3-E1 cells overexpressing *Hsc70* with ECH treatment. $n = 3, 5, 3, 4, 3$, and 3, respectively. (J) ALP activity quantification showing *Hsc70* overexpression blocking ECH-induced effects. $n = 3$. (K) ALP staining images of *Hsc70*-overexpressing MC3T3-E1 cells treated with ECH. Scale bar, 500 μm. $n = 3$. (L) Alizarin Red staining images demonstrating *Hsc70* overexpression reversing ECH-induced mineralization. Scale bar, 500 μm. $n = 3$. Data are expressed as means ± SD. $^{***}P < 0.001$, $^{**}P < 0.01$, $^{*}P < 0.05$ *vs* Control. ns, not significant.

3.6. hsc70 knockout alleviates prednisolone-induced OP in a zebrafish model

The zebrafish (*Danio rerio*) has become a powerful and versatile vertebrate model organism in a wide range of biomedical research areas, owing to its unique experimental advantages [27,28]. The glucocorticoid-induced zebrafish model is a well-established and widely used system for studying OP [29]. First, we assessed the effects of ECH on Pre-induced OP in zebrafish. The results showed that ECH treatment effectively increased ALP activity and de-

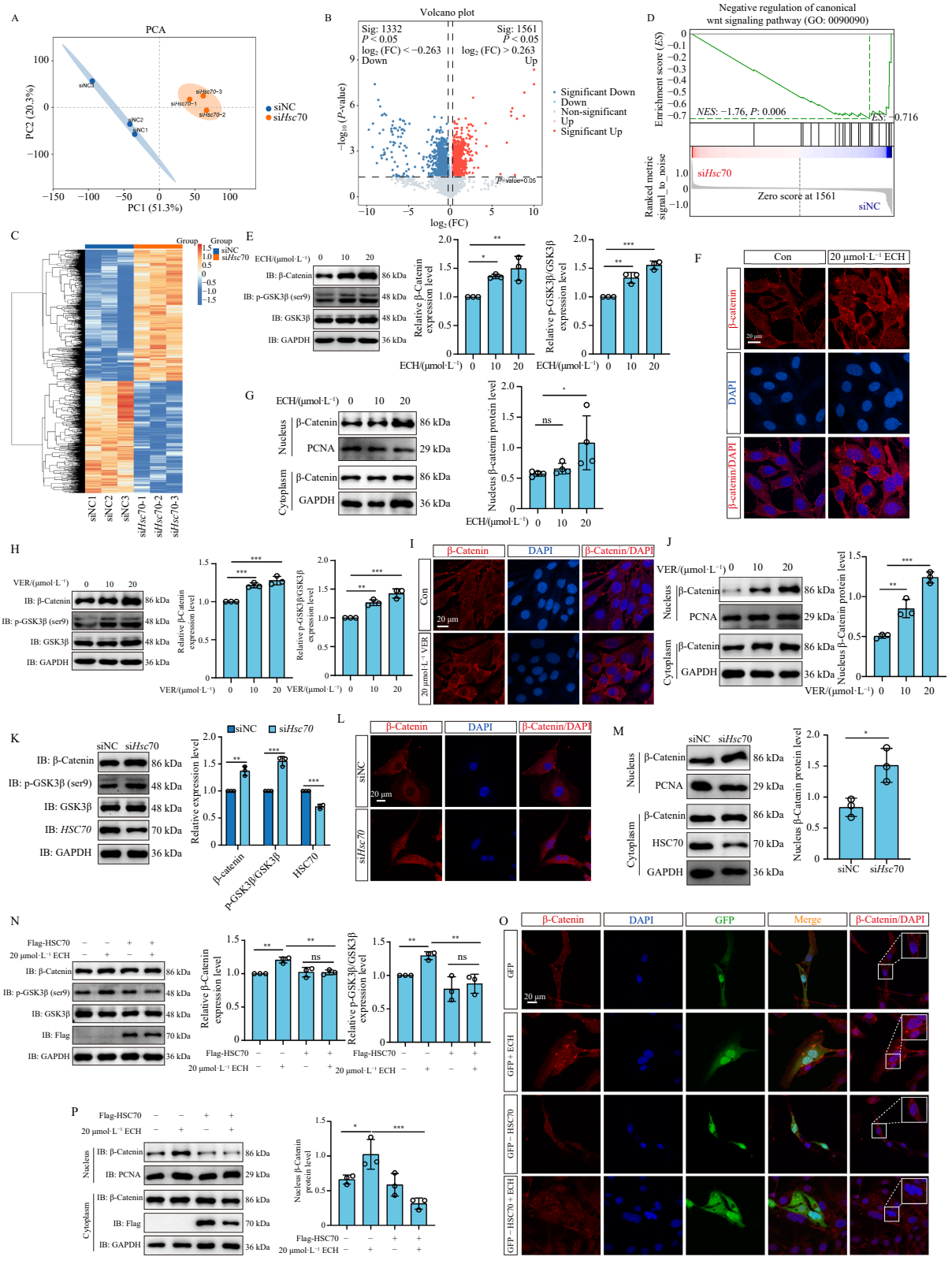

Fig. 4 HSC70 regulates osteoblast differentiation through the Wnt/β-catenin signaling pathway. (A) Principal component analysis (PCA) of experimental groups. (B) Volcano plot of differentially expressed proteins ($|\log_2(FC)| > 0.263$, $P < 0.05$) in *Hsc70*-knockdown MC3T3-E1 cells. (C) Heatmap of differentially expressed proteins ($P < 0.05$) in *Hsc70*-knockdown MC3T3-E1 cells. (D) GSEA of the "negative regulation of canonical Wnt signaling pathway" across groups. (E) WB analysis of β-catenin, GSK3β, and p-GSK3β (Ser9) in MC3T3-E1 cells treated with ECH for 72 h. $n = 3$. (F) Immunofluorescence staining of β-catenin nuclear translocation in ECH-treated MC3T3-E1 cells. Scale bar, 20 μm. (G) WB analysis of β-catenin nuclear translocation in ECH-treated MC3T3-E1 cells. $n = 4$. (H) WB analysis of β-catenin, GSK3β, and p-GSK3β (Ser9) in VER-155008-treated MC3T3-E1 cells. n = 3. (I) Immunofluorescence staining of β-catenin nuclear translocation in VER-155008-treated MC3T3-E1 cells. Scale bar, 20 μm. (J) Nuclear β-catenin levels in VER-155008-treated MC3T3-E1 cells analyzed by WB. $n = 3$. (K) WB analysis of β-catenin, GSK3β, and p-GSK3β (Ser9) in *Hsc70*-knockdown MC3T3-E1 cells. $n = 3$. (L) Immunofluorescence staining of β-catenin nuclear translocation in *Hsc70*-knockdown MC3T3-E1 cells. Scale bar, 20 μm. (M) Nuclear β-catenin levels in *Hsc70*-knockdown MC3T3-E1 cells analyzed by WB. $n = 3$. (N) WB analysis of β-catenin, GSK3β, and p-GSK3β (Ser9) in *Hsc70*-overexpressing MC3T3-E1 cells treated with ECH. $n = 3$. (O) Immunofluorescence staining of β-catenin nuclear translocation in *Hsc70*-overexpressing MC3T3-E1 cells treated with ECH. Scale bar, 20 μm. (P) Nuclear β-catenin levels in *Hsc70*-overexpressing MC3T3-E1 cells treated with ECH analyzed by western blot. $n = 3$. Data are expressed as means ± SD. $^{***}P < 0.001$, $^{**}P < 0.01$, $^{*}P < 0.05$ *vs* Control. ns, not significant.

creased tartrate-resistant acid phosphatase (TRAP) activity (Figs. 6A–6C). Alizarin Red staining further demonstrated that ECH significantly enhanced the mineralization area and integrated optical density (IOD) in Pre-induced OP zebrafish, indicating improved bone formation (Figs. 6D, 6E). Next, we investigated the effects of *hsc70* knockout (KO) on Pre-induced OP in zebrafish. Intriguingly, *hsc70* KO significantly reversed the Pre-induced reductions in ALP activity and the elevation of TRAP activity (Figs. 6F–6H). Consistently, compared with wild-type (WT) controls, *hsc70* KO restored the mineralization area and IOD in Pre-treated zebrafish (Figs. 6I, 6J). In summary, these data indicate that *hsc70* KO alleviates Pre-induced OP phenotypes in zebrafish, supporting a role for HSC70 as a negative regulator in bone health.

4. Discussion

OP is a multifactorial metabolic bone disorder characterized by an imbalance between bone resorption and bone formation [2, 30-32]. Although current pharmacological interventions primarily aim to either inhibit osteoclast activity or stimulate osteoblast function, their clinical efficacy is often limited, and long-term safety concerns remain [33-35]. Therefore, identifying novel therapeutic targets that can restore bone homeostasis is of significant importance. In the present study, we identified HSC70 as a negative regulator of osteoblast differentiation and demonstrated that ECH alleviates OP by directly targeting HSC70, thereby activating Wnt/β-catenin signaling and improving mitochondrial function.

Previous studies have mainly associated HSC70 with protein quality control and autophagy [5, 36-38], with emerging evidence suggesting its involvement in osteoclastogenesis and bone resorption [7, 8]. However, the role of HSC70 in osteoblast differentiation has remained unclear. Our results demonstrate that HSC70 ex-

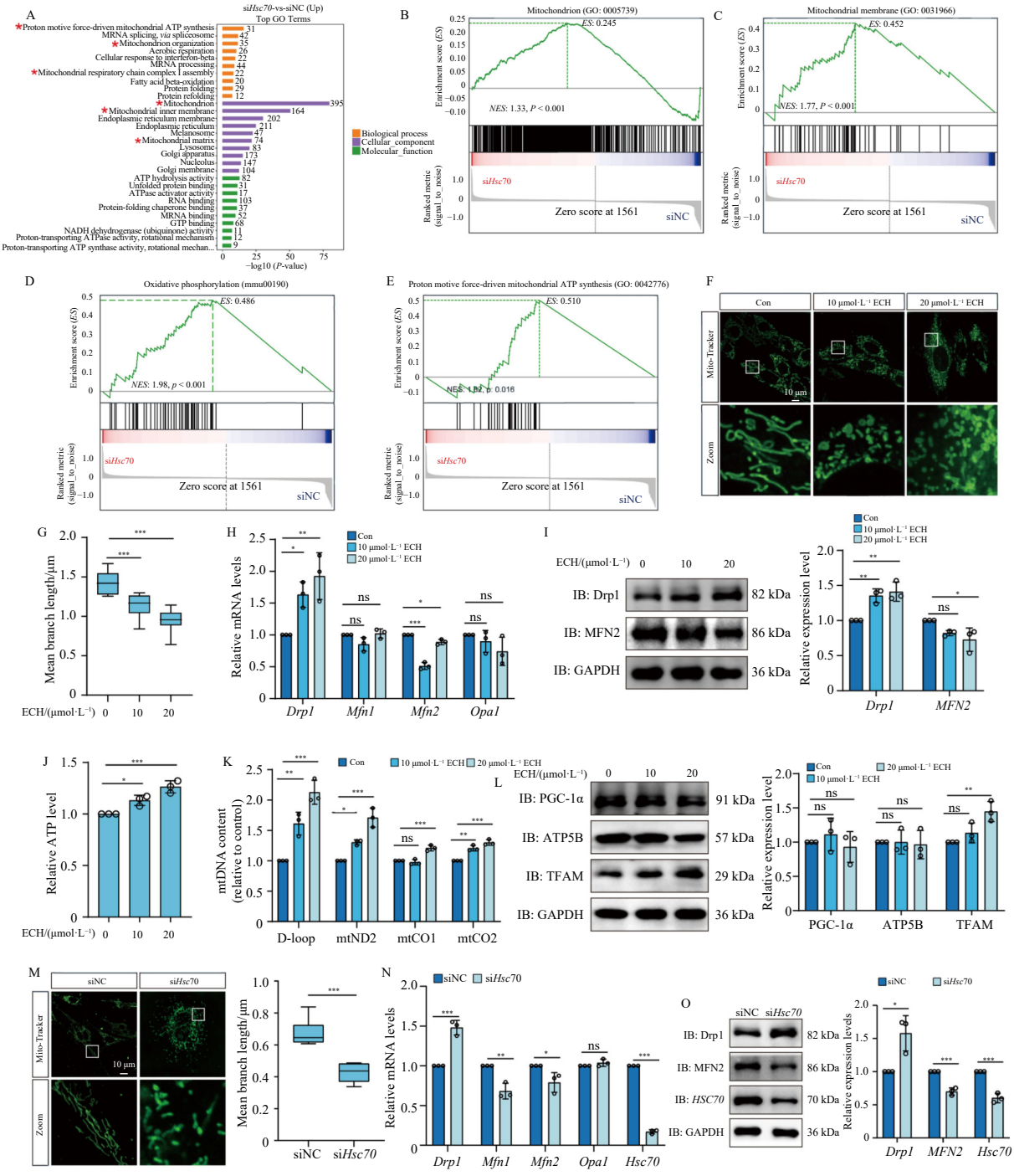

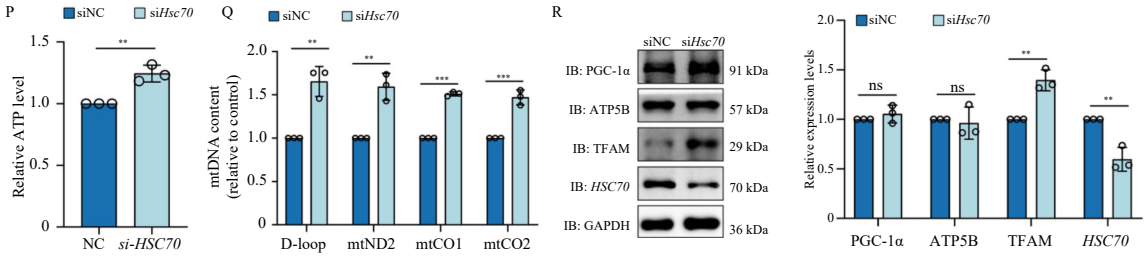

Fig. 5 HSC70 regulates mitochondrial homeostasis for osteoblast differentiation. (A) GO enrichment analysis of differentially expressed proteins in *Hsc70*-knockdown MC3T3-E1 cells. (B) GSEA of mitochondrion. (C) GSEA of mitochondrial membrane. (D) GSEA of oxidative phosphorylation. (E) GSEA of proton motive force-driven mitochondrial ATP synthesis. (F-G) Mitochondrial morphology analysis by Mito-Tracker staining showing reduced branch length in ECH-treated MC3T3-E1 cells. Scale bar, 10 μm. n = 3. (H) qRT-PCR quantification of *Drp1*, *Mfn1*, *Mfn2*, and *Opa1* mRNA levels in ECH-treated MC3T3-E1 cells. n = 3. (I) WB analysis of Drp1 and MFN2 protein levels in ECH-treated MC3T3-E1 cells. n = 3. (J) ATP production assay in ECH-treated MC3T3-E1 cells. n = 3. (K) Mitochondrial DNA (mtDNA) content quantification by qRT-PCR in ECH-treated cells. n = 3. (L) WB analysis of PGC-1α, ATP5B, and TFAM protein levels in ECH-treated MC3T3-E1 cells. n = 3. (M) Mitochondrial morphology analysis by Mito-Tracker staining showing reduced branch length in *Hsc70*-knockdown MC3T3-E1 cells. Scale bar, 10 μm. n = 3. (N) qRT-PCR quantification of *Drp1*, *Mfn1*, *Mfn2*, and *Opa1* mRNA levels in *Hsc70*-knockdown MC3T3-E1 cells. n = 3. (O) WB analysis of Drp1 and MFN2 protein levels in *Hsc70*-knockdown MC3T3-E1 cells. n = 3. (P) ATP production assay in *Hsc70*-knockdown MC3T3-E1 cells. n = 3. (Q) mtDNA content quantification by qRT-PCR in *Hsc70*-knockdown MC3T3-E1 cells. n = 3. (R) WB analysis of PGC-1α, ATP5B, and TFAM protein levels in *Hsc70*-knockdown MC3T3-E1 cells. n = 3. Data are expressed as means ± SD. $^{***}P < 0.001$, $^{**}P < 0.01$, $^{*}P < 0.05$ *vs* Control. ns, not significant.

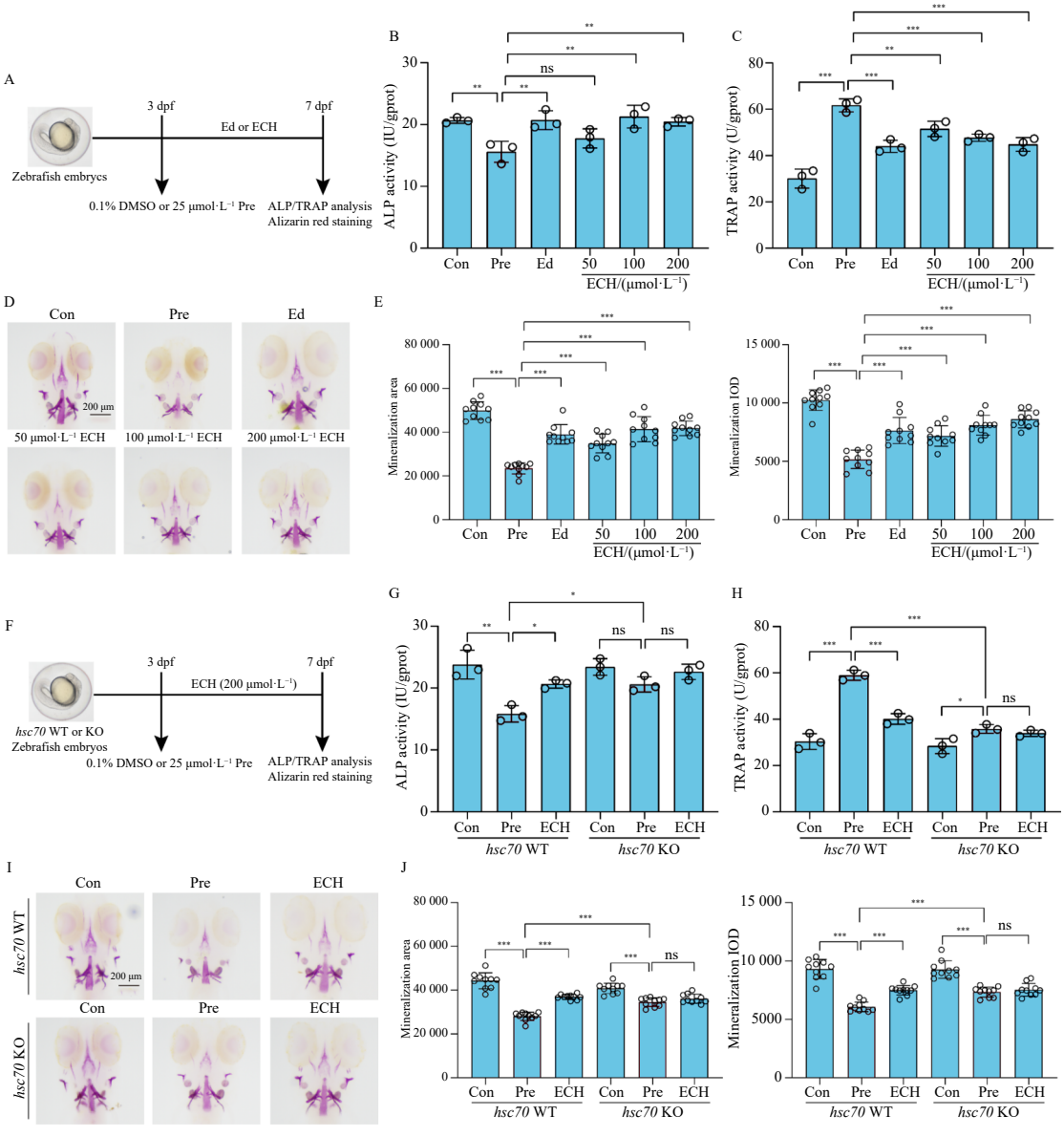

Fig. 6 *hsc70* knockout alleviates prednisolone-induced OP in a zebrafish model. (A) Schematic of the experimental design for evaluating ECH efficacy in a glucocorticoid-induced OP zebrafish model. (B) ALP activity in ECH-treated OP zebrafish. n = 3. (C) TRAP activity in ECH-treated OP zebrafish. n = 3. (D) Representative Alizarin Red staining of zebrafish larval mineralization across experimental groups. (E) Quantification of mineralization area and integrated optical density (IOD) from panel D. n = 10 larvae/group. (F) Experimental design for assessing *hsc70* knockout (KO) effects in OP zebrafish model. (G) Effect of *hsc70* KO on ALP activity in zebrafish model of OP. n = 3. (H) Effect of *hsc70* KO on TRAP activity in zebrafish model of OP. n = 3. (I) Representative Alizarin Red staining of zebrafish larval mineralization in *hsc70* WT and *hsc70* KO groups. (J) Quantification of mineralization area and IOD from panel I. n = 10 larvae/group. Data are expressed as means ± SD. $^{***}P < 0.001$, $^{**}P < 0.01$, $^{*}P < 0.05$ *vs* Control. ns, not significant.

erts an inhibitory effect on osteoblast differentiation by repressing β-catenin activity and perturbing mitochondrial homeostasis. This finding extends the biological significance of HSC70 to skeletal regulation and highlights its dual role as both a molecular chaperone and a metabolic checkpoint in bone biology. Importantly, inhibition or knockdown of HSC70 recapitulated the effects of ECH, validating HSC70 as a druggable target for bone-anabolic therapy.

The identification of ECH as a natural inhibitor of HSC70 further enriches its pharmacological profile. ECH has been reported to inhibit osteoclast activity [18-20], protect neuronal cells [16, 17, 39], and exert anti-inflammatory effects [16, 40]. Here, we show that ECH promotes osteoblast differentiation by simultaneously activating Wnt/β-catenin signaling and enhancing mitochondrial function. This dual regulation is particularly relevant, as osteoblast differentiation is energy-intensive and tightly coupled to mitochondrial metabolism [41-43]. By improving mitochondrial dynamics and biogenesis, ECH ensures adequate bioenergetic support for osteogenesis. These findings support the concept that natural products such as ECH can serve as multi-target modulators, bridging signaling pathways with metabolic regulation.

It is noteworthy that the regulatory role of HSC70 in Wnt/β-catenin signaling appears to be context-dependent. In certain cancer models, HSC70 activation facilitates β-catenin signaling and tumor progression [44], whereas in osteoblasts, our data show that HSC70 represses β-catenin nuclear translocation. This discrepancy may arise from the differential availability of HSC70 co-chaperones or interacting proteins across distinct cellular environments. Understanding these cell type-specific interactions may guide the development of selective HSC70-targeted therapies with minimal off-target effects.

Mitochondrial remodeling emerged as another critical downstream event of HSC70 inhibition. Although excessive mitochondrial fission is often associated with dysfunction [45], our findings indicate that moderate remodeling, characterized by increased fission coupled with enhanced biogenesis, can support osteoblast differentiation. These results align with previous studies showing that dynamic mitochondrial changes promote energy output and favor osteogenic lineage commitment [46, 47]. Furthermore, the observed crosstalk between β-catenin signaling and mitochondrial regulation suggests a tightly coordinated mechanism in which transcriptional programming and metabolic adaptation synergize to drive bone formation.

From a translational perspective, these findings position HSC70 as a promising therapeutic target for OP. Pharmacological inhibition of HSC70 by ECH not only restores osteoblast function but also addresses mitochondrial dysfunction, a pathological hallmark of glucocorticoid-induced and age-related bone loss [30-32]. The zebrafish OP model provided compelling *in vivo* validation, as both ECH treatment and *hsc70* knockout significantly improved bone mineralization. These results underscore the therapeutic potential of targeting the HSC70–β-catenin/mitochondria axis in OP and possibly in other metabolic bone disorders.

Nonetheless, several limitations should be acknowledged. First, although zebrafish models provided valuable *in vivo* insights, further validation in mammalian systems, particularly rodent models of postmenopausal or glucocorticoid-induced OP, is required. Second, because ECH is a multitarget natural compound [48], comprehensive profiling is necessary to assess potential off-target effects.

Taken together, our findings establish a previously unrecognized role of HSC70 as a negative regulator of osteoblast differentiation and identify ECH as a natural HSC70 inhibitor with bone-anabolic effects. By bridging Wnt/β-catenin signaling and mitochondrial homeostasis, ECH provides a multifaceted approach to restoring bone health. These insights open new avenues for developing innovative therapeutic strategies for OP and highlight the broader potential of targeting HSC70 in metabolic and degenerative diseases.

5. Conclusion

In summary, this study identifies HSC70 as a novel negative regulator of osteoblast differentiation and demonstrates that ECH directly targets HSC70 to restore bone homeostasis. By inhibiting HSC70, ECH activates Wnt/β-catenin signaling and enhances mitochondrial function, thereby promoting osteoblast differentiation and mitigating OP phenotypes. These findings establish the HSC70–β-catenin/mitochondrial axis as a druggable pathway and highlight ECH as a promising natural lead for developing bone-anabolic therapies.

Funding

This study was supported by the National Natural Science Foundation of China (No. 82322072), the Key Research and Development Program of Xinjiang Uygur Autonomous Region (No. 2023B03012-1), and the Fundamental Research Funds for the Central Universities (No. 2632025TD06).

Declaration of competing interests

These authors have no conflict of interest to declare.

References

1 Yang TL, Shen H, Liu A, et al. A road map for understanding molecular and genetic determinants of osteoporosis. *Nat Rev Endocrinol*. 2020;16(2):91-103. https://doi.org/10.1038/s41574-019-0282-7.
2 Raisz LG. Pathogenesis of osteoporosis: concepts, conflicts, and prospects. *J Clin Invest*. 2005;115(12):3318-25. https://doi.org/10.1172/JCI27071.
3 Reid IR, Billington EO. Drug therapy for osteoporosis in older adults. *Lancet*. 2022;399(10329):1080-1092. https://doi.org/10.1016/S0140-6736(21)02646-5.
4 Brent MB. Pharmaceutical treatment of bone loss: from animal models and drug development to future treatment strategies. *Pharmacol Ther*. 2023;244:108383. https://doi.org/10.1016/j.pharmthera.2023.108383.
5 Stricher F, Macri C, Ruff M, et al. HSPA8/HSC70 chaperone protein: structure, function, and chemical targeting. *Autophagy*. 2013;9(12):1937-1954. https://doi.org/10.4161/auto.26448.
6 Liu T, Daniels CK, Cao S. Comprehensive review on the HSC70 functions, interactions with related molecules and involvement in clinical diseases and therapeutic potential. *Pharmacol Ther*. 2012;136(3):354-374. https://doi.org/10.1016/j.pharmthera.2012.08.014.
7 Li Q, Yue T, Du X, et al. HSC70 mediated autophagic degradation of oxidized PRL2 is responsible for osteoclastogenesis and inflammatory bone destruction. *Cell Death Differ*. 2023;30(3):647-659. https://doi.org/10.1038/s41418-022-01068-y.
8 Notsu K, Nakagawa M, Nakamura M. Ubiquitin-like protein MNSFbeta noncovalently binds to molecular chaperone HSPA8 and regulates osteoclastogenesis. *Mol Cell Biochem*. 2016;421(1-2):149-156. https://doi.org/10.1007/s11010-016-2795-x.
9 Li X, Huang M, Zheng H, et al. CHIP promotes Runx2 degradation and negatively regulates osteoblast differentiation. *J Cell Biol*. 2008;181(6):959-972. https://doi.org/10.1083/jcb.200711044.
10 Xie J, Gu J. Identification of C-terminal Hsp70-interacting protein as a mediator of tumour necrosis factor action in osteoblast differentiation by targeting osterix for degradation. *J Cell Mol Med*. 2015;19(8):1814-1824. https://doi.org/10.1111/jcmm.12553.
11 Wang W, Li J, Ko FC, et al. CHIP regulates skeletal development and postnatal bone growth. *J Cell Physiol*. 2020;235(6):5378-5385. https://doi.org/10.1002/jcp.29424.
12 Greenhough J, Papadakis ES, Cutress RI, et al. Regulation of osteoblast development by Bcl-2-associated athanogene-1 (BAG-1). *Sci Rep*. 2016;6:33504. https://doi.org/10.1038/srep33504.
13 Jiang Y, Tu PF. Analysis of chemical constituents in Cistanche species. *J Chromatogr A*. 2009;1216(11):1970-1979. https://doi.org/10.1016/j.chroma.2008.07.031.
14 Li J, Yu H, Yang C, et al. Therapeutic potential and molecular mechanisms of echinacoside in neurodegenerative diseases. *Front Pharmacol*. 2022;13:841110. https://doi.org/10.3389/fphar.2022.841110.
15 Wang W, Jiang S, Zhao Y, et al. Echinacoside: a promising active natural products and pharmacological agents. *Pharmacol Res*. 2023;197:106951. https://doi.org/10.1016/j.phrs.2023.106951.
16 Li X, Zhang X, Yuan X, et al. Echinacoside mitigates sepsis-associated encephalopathy by inhibiting STING pathway and reducing neuroinflammation. *Eur J Pharmacol*. 2025;1005:178092. https://doi.org/10.1016/j.ejphar.2025.178092.

17 Yang Z, Zhao Y, Wang Y, et al. Echinacoside ameliorates post-stroke depression by activating BDNF signaling through modulation of Nrf2 acetylation. *Phytomedicine*. 2024;128:155433. https://doi.org/10.1016/j.phymed.2024.155433.
18 Jiang T, Gu H, Wei J. Echinacoside inhibits osteoclast function by down-regulating PI3K/Akt/C-Fos to alleviate osteolysis caused by periprosthetic joint infection. *Front Pharmacol*. 2022;13:930053. https://doi.org/10.3389/fphar.2022.930053.
19 Hu D, Cheng C, Bian Z, et al. The role of echinacoside-based cross-linker nanoparticles in the treatment of osteoporosis. *PeerJ*. 2024;12:e17229. https://doi.org/10.7717/peerj.17229.
20 Yi Q, Sun M, Jiang G, et al. Echinacoside promotes osteogenesis and angiogenesis and inhibits osteoclast formation. *Eur J Clin Invest*. 2024;54(8):e14198. https://doi.org/10.1111/eci.14198.
21 Li F, Yang Y, Zhu P, et al. Echinacoside promotes bone regeneration by increasing OPG/RANKL ratio in MC3T3-E1 cells. *Fitoterapia*. 2012;83(8):1443-1450. https://doi.org/10.1016/j.fitote.2012.08.008.
22 Li F, Yang X, Yang Y, et al. Antiosteoporotic activity of echinacoside in ovariectomized rats. *Phytomedicine*. 2013;20(6):549-557. https://doi.org/10.1016/j.phymed.2013.01.001.
23 Chen Y, Li YQ, Fang JY, et al. Establishment of the concurrent experimental model of osteoporosis combined with Alzheimer's disease in rat and the dual-effects of echinacoside and acteoside from *Cistanche tubulosa*. *J Ethnopharmacol*. 2020;257:112834. https://doi.org/10.1016/j.jep.2020.112834.
24 Rix U, Superti-Furga G. Target profiling of small molecules by chemical proteomics. *Nat Chem Biol*. 2009;5(9):616-624. https://doi.org/10.1038/nchembio.216.
25 Chopra B, Dhingra AK. Natural products: a lead for drug discovery and development. *Phytother Res*. 2021;35(9):4660-4702. https://doi.org/10.1002/ptr.7099.
26 Westerfield M. The zebrafish book: a guide for the laboratory use of zebrafish (*Danio rerio*). University of Oregon Press; 2007.
27 Goldsmith P. Zebrafish as a pharmacological tool: the how, why and when. *Curr Opin Pharmacol*. 2004;4(5):504-512. https://doi.org/10.1016/j.coph.2004.04.005.
28 Barros TP, Alderton WK, Reynolds HM, et al. Zebrafish: an emerging technology for *in vivo* pharmacological assessment to identify potential safety liabilities in early drug discovery. *Br J Pharmacol*. 2008;154(7):1400-1413. https://doi.org/10.1038/bjp.2008.249.
29 Barrett R, Chappell C, Quick M, et al. A rapid, high content, *in vivo* model of glucocorticoid-induced osteoporosis. *Biotechnol J*. 2006;1(6):651-655. https://doi.org/10.1002/biot.200600043.
30 Song S, Guo Y, Yang Y, et al. Advances in pathogenesis and therapeutic strategies for osteoporosis. *Pharmacol Ther*. 2022;237:108168. https://doi.org/10.1016/j.pharmthera.2022.108168.
31 Chotiyarnwong P, McCloskey EV. Pathogenesis of glucocorticoid-induced osteoporosis and options for treatment. *Nat Rev Endocrinol*. 2020;16(8):437-447. https://doi.org/10.1038/s41574-020-0341-0.
32 Zhivodernikov IV, Kirichenko TV, Markina YV, et al. Molecular and cellular mechanisms of osteoporosis. *Int J Mol Sci*. 2023;24(21):15772. https://doi.org/10.3390/ijms242115772.
33 Compston JE, McClung MR, Leslie WD. Osteoporosis. *Lancet*. 2019;393(10169):364-376. https://doi.org/10.1016/S0140-6736(18)32112-3.
34 Cheng C, Wentworth K, Shoback DM. New frontiers in osteoporosis therapy. *Annu Rev Med*. 2020;71:277-288. https://doi.org/10.1146/annurev-med-052218-020620.
35 Adejuyigbe B, Kallini J, Chiou D, et al. Osteoporosis: molecular pathology, diagnostics, and therapeutics. *Int J Mol Sci*. 2023;24(19):14583. https://doi.org/10.3390/ijms241914583.
36 Lin J, Wei X, Dai Y, et al. Chaperone-mediated autophagy degrades SERPINA1 (E342K)/alpha1-antitrypsin Z variant and alleviates cell stress. *Autophagy*. 2025;21(8):1662-1679. https://doi.org/10.1080/15548627.2025.2480037.
37 Wu Z, Yang S, Jiang Z, et al. UCHL1 alleviates nucleus pulposus cell senescence by promoting chaperone-mediated autophagy antagonizing autophagy-dependent ferroptosis through deubiquitination of HSPA8. *Autophagy*. 2025;21:1-25. https://doi.org/10.1080/15548627.2025.2544287.
38 Zhang G, Xiang M, Gu L, et al. The essential role of TTC28 in maintaining chromosomal stability *via* HSPA8 chaperone-mediated autophagy. *Proc Natl Acad Sci U S A*. 2024;121(50):e2409447121. https://doi.org/10.1073/pnas.2409447121.
39 Yang XP, Huang JH, Ye FL, et al. Echinacoside exerts neuroprotection *via* suppressing microglial alpha-synuclein/TLR2/NF-kappaB/NLRP3 axis in parkinsonian models. *Phytomedicine*. 2024;123:155230. https://doi.org/10.1016/j.phymed.2023.155230.
40 Wang H, Bian Y, Li Y, et al. Echinacoside: a potential therapeutic approach for alcohol-related liver disease by alleviating intestinal microbial dysbiosis, intestinal barrier dysfunction, and liver inflammation mediated by the endotoxin-TLR4/NF-kappaB pathway. *Eur J Pharmacol*. 2025;1005:178027. https://doi.org/10.1016/j.ejphar.2025.178027.
41 Pei L, Yao Z, Liang D, et al. Mitochondria in skeletal system-related diseases. *Biomed Pharmacother*. 2024;181:117505. https://doi.org/10.1016/j.biopha.2024.117505.
42 Yu F, Zhao X, Jiang T, et al. Enhancing osteogenesis through bio-inspired recombinant coral protein galaxin by targeting mitochondrial metabolism and ATP production. *Adv Sci (Weinh)*. 2025;12(17):e2412867. https://doi.org/10.1002/advs.202412867.
43 He Y, Liu T, Peng X, et al. Molecular mechanism of mitochondrial autophagy mediating impaired energy metabolism leading to osteoporosis. *Biochim Biophys Acta Mol Basis Dis*. 2025;1871(3):167685. https://doi.org/10.1016/j.bbadis.2025.167685.
44 Li B, Ming H, Qin S, et al. HSPA8 activates Wnt/beta-catenin signaling to facilitate BRAF V600E colorectal cancer progression by CMA-mediated CAV1 degradation. *Adv Sci (Weinh)*. 2024;11(3):e2306535. https://doi.org/10.1002/advs.202306535.
45 Chen W, Zhao H, Li Y. Mitochondrial dynamics in health and disease: mechanisms and potential targets. *Signal Transduct Target Ther*. 2023;8(1):333. https://doi.org/10.1038/s41392-023-01547-9.
46 Suh J, Kim NK, Shim W, et al. Mitochondrial fragmentation and donut formation enhance mitochondrial secretion to promote osteogenesis. *Cell Metab*. 2023;35(2):345-360.e7. https://doi.org/10.1016/j.cmet.2023.01.003.
47 Ling Z, Ge X, Jin C, et al. Copper doped bioactive glass promotes matrix vesicles-mediated biomineralization *via* osteoblast mitophagy and mitochondrial dynamics during bone regeneration. *Bioact Mater*. 2025;46:195-212. https://doi.org/10.1016/j.bioactmat.2024.12.010.
48 Zeng KW, Wang JK, Wang LC, et al. Small molecule induces mitochondrial fusion for neuroprotection *via* targeting CK2 without affecting its conventional kinase activity. *Signal Transduct Target Ther*. 2021;6(1):71. https://doi.org/10.1038/s41392-020-00447-6.

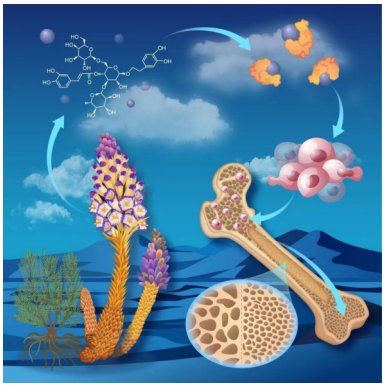

This cover illustrates the translational discovery of echinacoside (ECH), a bioactive phenylethanoid glycoside from the desert medicinal plant *Cistanche deserticola*, as a promising natural therapeutic candidate for osteoporosis (OP). OP, a prevalent skeletal disorder driven by impaired osteoblast function and excessive bone resorption, remains in urgent need of safe and effective anabolic therapies. In this work, we identify heat shock cognate 71 kDa protein (HSC70) as a novel negative regulator of osteoblast differentiation, and reveal ECH as its direct pharmacological inhibitor. As visually depicted in the artwork, ECH binds to HSC70 to block its suppressive function, triggering a cascade of osteogenic events: activation of the canonical Wnt/β-catenin pathway, enhanced β-catenin nuclear translocation, and improved mitochondrial dynamics, ATP production, and biogenesis. These effects collectively provide robust metabolic support for osteoblast maturation and bone mineralization. *In vivo*, both ECH administration and *hsc70* knockout alleviated glucocorticoid-induced bone loss and restored healthy bone microarchitecture in zebrafish models. This study uncovers the druggable HSC70-β-catenin/mitochondrial axis for skeletal homeostasis, positioning ECH as a lead natural compound for developing novel anti-osteoporotic therapies. The visual narrative traces this journey from the source plant and its active molecule, through target engagement and cellular signaling, to the restoration of bone health.